Limnol. Oceanogr., 50(4), 2005, 1326–1333

The internal wave field in Sau reservoir: Observation and modeling of a third vertical mode

Javier Vidal, Xavier Casamitjana,[1] *Jordi Colomer, and Teresa Serra*
Department of Physics and Institute of Environmental Sciences, University of Girona, Catalonia, Spain

Abstract

Water withdrawal from Mediterranean reservoirs in summer is usually very high. Because of this, stratification is often continuous and far from the typical two-layered structure, favoring the excitation of higher vertical modes. The analysis of wind, temperature, and current data from Sau reservoir (Spain) shows that the third vertical mode of the internal seiche (baroclinic mode) dominated the internal wave field at the beginning of September 2003. We used a continuous stratification two-dimensional model to calculate the period and velocity distribution of the various modes of the internal seiche, and we calculated that the period of the third vertical mode is ~24 h, which coincides with the period of the dominating winds. As a result of the resonance between the third mode and the wind, the other oscillation modes were not excited during this period.

Standing internal waves, or seiches, are a ubiquitous feature of lakes, existing mainly as a result of the wind force acting on a stratified water column. Internal seiches are important for many processes in lakes and reservoirs. Part of the kinetic energy introduced at the water surface by the wind is transferred to internal seiches and becomes available for mixing. Imberger (1998) and Wüest et al. (2000) showed that most of the momentum and energy that passes through the surface mixed layer and enters the interior is transferred to internal wave motions. This energy is typically about 10% of the total wind energy input into the lake (Wüest and Lorke 2003). The vertical excursions of fluid associated with the wave motions have been shown to affect the spatial distribution of different organisms (Levy et al. 1991). The bottom currents induced by internal seiches contribute to the mixing and resuspension of sediments in the benthic boundary layer (Gloor et al. 1994). MacManus and Duck (1988) showed that seiche-induced resuspension was responsible for sediment scouring patterns observed along the sides of Loch Earn. Therefore, given that internal seiches play a significant role in a broad range of physical, chemical, and biological processes, there is a lot of interest in their assessment and evaluation.

Although there are many possible mechanisms that induce seiches, like air-pressure fluctuations, earthquakes, etc., it is mainly the lake's response to the wind forcing that causes the seiche excitation. The wind forcing in lakes is often periodic because of the periodicity in weather patterns. Wind applied to the surface can cause a surface set-up of water at the downwind end. This pressure force is balanced by the metalimnion tilting in the opposite sense—that is, downward at the downwind end (Spiegel and Imberger 1980). When the wind forcing relaxes the water surface oscillates, as does the metalimnion. The so-called external seiche is the oscillation of the water surface (a barotropic mode), whereas the internal seiche (baroclinic mode) is the oscillation of the metalimnion. In large lakes the picture becomes more complicated because of the effects of the Earth's rotation (Antenucci and Imberger 2003).

Internal seiches can be divided into different categories, depending on the nodal points (ViHj), where i and j are the number of vertical and horizontal nodes (Fig. 1). The most commonly observed, the V1H1, has one vertical and one horizontal nodal point. This kind of standing wave results when the metalimnion's thickness is small and when the lake can be approximated by a two-layer body. Medium- or large-sized lakes often have a temperature profile that makes reasonable the two- or three-layer approximation. However, the temperature profile of many reservoirs is very far from the typical three-layer pattern (Casamitjana et al. 2003). This is mostly the result of the high demand for water in summer, which contributes to the creation of an additional stratification where the outlet structures of the reservoir are located. Surface mixing phenomena together with water withdrawal and the development of internal seiches create a vertical thermal structure where temperature gradients of different intensities are found.

When the internal waves have periods of similar magnitude to the wind, the possibility of resonant forcing should be taken into account. In two- or three-layer structures the frequency spectrum is discrete, but in a continuous stratification structure, the spectrum is dense, and any forcing frequency can lead to resonance seiching (Münnich 1996). However, the resonant modes can have such a high order of structures that in practice they are never excited. This is because of the dampening produced by the large amount of shear existing in higher modes. Anntenucci et al. (2000) presented evidence of the resonant forcing of a Kelvin wave in Lake Kinneret, which, during the time at which it was measured, had a period of ~24 h, coinciding with the wind forcing return period over the lake.

Although observations of higher horizontal modes along with the first vertical mode are not unusual in lakes (*see,* for

[1] Corresponding author (xavier.casamitjana@udg.es).

Acknowledgments

This work was supported by the Spanish government (MCYT) and the European Union (FEDER) through the REM2001-2239 project. We thank the Catalan Water Agency and Aigües Ter-Llobregat for their support throughout the campaign. We also thank Joan Armengol for his unconditional support and two unknown reviewers for their constructive reviews of the original manuscript.

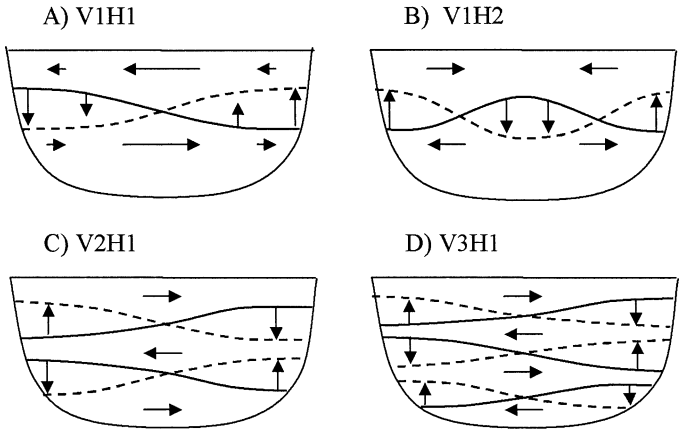

Fig. 1. Schematic view of various seiche modes in a closed basin. The notation used to characterize the mode takes the form ViHj = *i*th vertical, *j*th horizontal mode. Vertical and horizontal vectors show the direction of flow between an initial state of maximum vertical displacement (continuous line) and one half period later (dashed line).

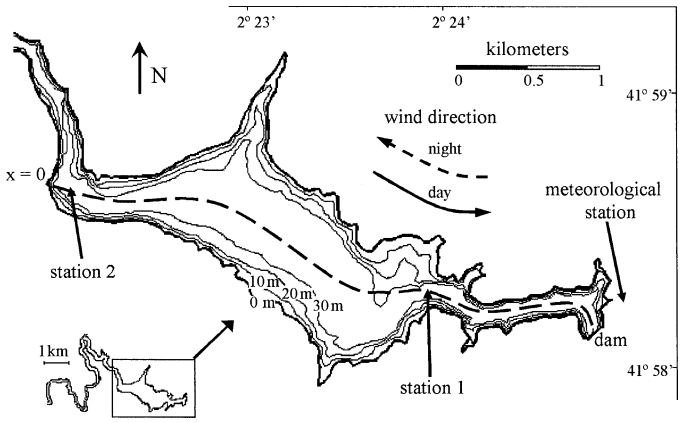

Fig. 2. Bathymetric map of Sau Reservoir showing the location of the measuring stations and the meteorological station. The dotted line represents the main axis of the reservoir (x) and the direction in which the wind velocity and the water currents are projected.

example, Lemmin and Mortimer 1986), higher vertical modes are more rarely reported. Second vertical modes have been reported by LaZerte (1980), Wiegan and Chamberlain (1987), Münnich et al. (1992), and Roget et al. (1997). Münnich et al. (1992) showed that the second vertical mode V2H1 is dominant in the wave field of Alpnacher See, a side basin of Lake Lucerne, and that resonance with diurnal wind is responsible for the high amplitudes of the mode. Until now, the only experimental evidence of a third vertical mode has been reported by Perez et al. (2003), whose measurements, carried out with a thermistor string, show the existence of four layers oscillating with a 24-h period. However, in their study they did not describe whether the oscillating mode was an eigenvalue to the actual stratification.

In the present article we present experimental evidence of a third vertical mode with a period of ~24 h occurring in a Spanish reservoir. This mode was found to dominate the internal wave field during the first days of September 2003, when the stratification was fully developed. In addition, the modeling of the reservoir wave field shows us that the third mode is an eigenvalue, with the same period as the wind. Given that the natural and the forcing frequencies coincide, we conclude that resonance between the wind and the third mode is responsible of the minor excitation of other modes like the V1H1, which can be found in the wave field of the reservoir during other periods: for example, at the end of July 2003.

Materials and methods

Study site—Sau is a canyon-shaped reservoir, 18.225 km long, situated in the central part of the river Ter, which is 200 km long, with its source in the Pyrenees in the northeast of Spain (Fig. 2). However, the length of the lacustrine part of the reservoir is 3,600 m, and the maximum width is 1,300 m (Armengol et al. 1999). The elongated geometry, along with the wind-driven forces following the canyon, encourage us to expect that the internal seiches follow the main axis of the reservoir. Here we present the results of different surveys carried out in July 2003 and September 2003 during the stratification period of the reservoir. An electromagnetic current meter (ECM), an acoustic Doppler current meter (ADCP), and a thermistor string (TS1) were deployed at station 1 (Sta. 1), while another thermistor string was deployed at Sta. 2 (ADCP: from 21–24 July and 9–17 September; ECM: from 9–17 September; TS1 from 21 July–20 August and 9 September–2 October; TS2 from 9 September–2 October).

The ADCP (RDI 600-kHz Workhorse Sentinel) was deployed in the water surface with the beams facing downward. In this way we were not able to get information about the water surface velocity, and, therefore, we also used an ECM (ACM8M, Alec Electronics). Data from the ADCP was received from 20 depth bins, each of which was 2 m high. The sampling rate was set at 1 Hz, with the raw data processed to obtain 7.5-min–averaged data, with a standard deviation of 0.1 cm s^{-1}. In the processed data, the bottom boundary layer was cut out because of the lack of confidence in the velocity, the result of bottom vegetation. The first depth bin was set at 3 m, and then a range between 3 and 30 m was processed. The ECM sampled the two components of the horizontal velocity at 2 Hz and was deployed 1 m from the water surface. The thermistor chain TS1 was composed of 11 thermistors placed at the following depths: 3, 4, 5, 6, 7, 8, 9, 11, 15, 16, and 17 m, whereas TS2 was composed of four thermistors regularly spaced between 5 m and 15 m. The sampling interval of both thermistor chains was 10 min.

Experimental evidence of the third mode—In summer, the habitual 24-h pattern for the wind is the one corresponding to the first 5 d in Fig. 3A. During the day, the wind blows toward the dam (Fig. 2) (i.e., a positive direction in Fig. 3A); during the night there is a slight breeze in the opposite direction. This happens with the prevalent summer anticyclonic conditions; however, from time to time the pattern is disrupted when storms come over. Wind and water velocities in Fig. 3 have been obtained by projecting their values in

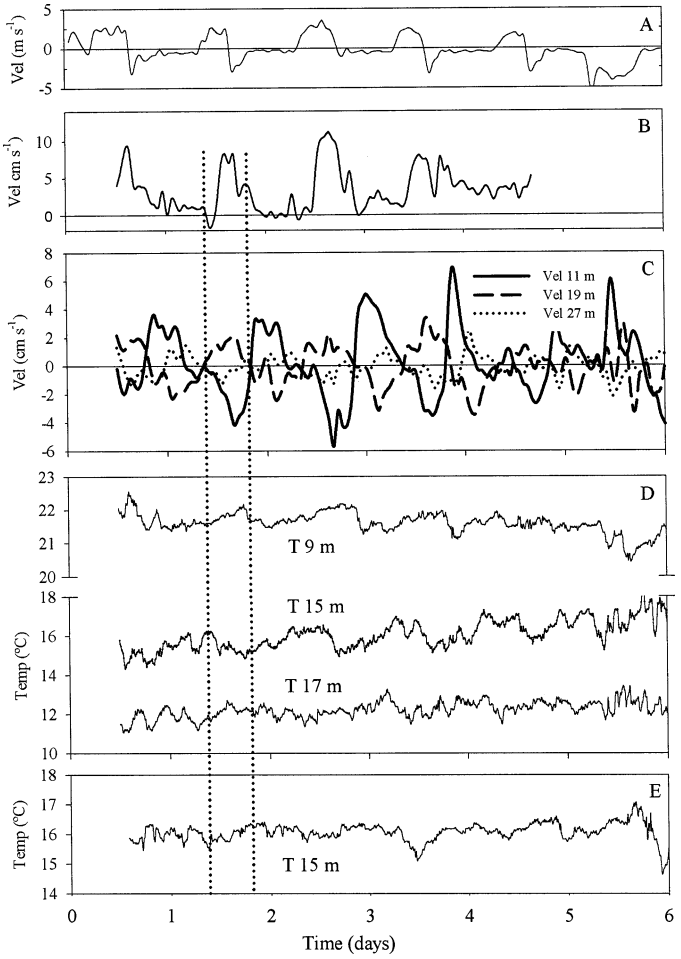

Fig. 3. (A) Wind velocity, (B) surface-water velocity, and (C) water velocity, projected following the main axis of the reservoir at Sta. 1 (*see Fig. 2*). Values of water velocity have been averaged at 1-h periods. (D) Water temperature measured by the thermistor string at Sta. 1 and (E) at Sta. 2. Day 0 corresponds to 9 September 2003. The dotted lines show the experimental evidence for mode V3H1.

the *x* direction (Fig. 2). Experimental data show that values perpendicular to the *x* direction are much less important. The wind velocity (Fig. 3A) has a strong correlation with the surface-water velocity (Fig. 3B). Most of the time the wind blows toward the dam and the surface water moves in the same direction. After the wind stops, there seems to be a residual water velocity toward the dam, and, finally, the velocity remains close to zero. Because of this, the velocity of Fig. 3B reflects the existence of a wind-driven current. The velocity at 19 m (Fig. 3C) follows a similar pattern to that of the surface-water velocity, although the surface layer velocity is nearly never negative. However, water velocities at 11 m and 27 m were out of phase, indicating that a third mode may take place. This is also evident when looking at Fig. 4A. Here, light and dark colors indicate currents in opposite directions (light: current toward the dam; dark: current from the dam). Water changes its direction between water layers two and three and four, as a consequence of the third mode. Water direction in the first layer, which roughly corresponds to the surface mixed layer, cannot be used in this line of argument because of the many physical processes occurring here, such as convection, wind stirring, etc., that can mask the third mode. In addition, in Fig. 4A it can be seen that there is a shifting in the velocity direction time series between the different layers. This shifting can be explained by the existing delay in the transmission of the momentum from the wind between the layers. Figure 4B shows the temperature profile measured on 9 September near the middle of the reservoir, where the vertical displacements of the H1 modes are assumed to be small (Fig. 1). The stratification profile of Fig. 4B shows a four-layer structure, which corresponds approximately to the four-layer structure of the velocity field (Fig. 4A) that could favor the development of the third vertical mode.

The third mode can also be observed when looking at temperature measurements in Fig. 3D. Here the temperature at 15 m is in the opposite phase compared to the temperatures at 9 m and 17 m, indicating the vertical displacements of the three interface layers. Unfortunately, we were not able to look at deeper depths because of the length of the thermistor string. The temperature at 15 m at Sta. 2 is also in the

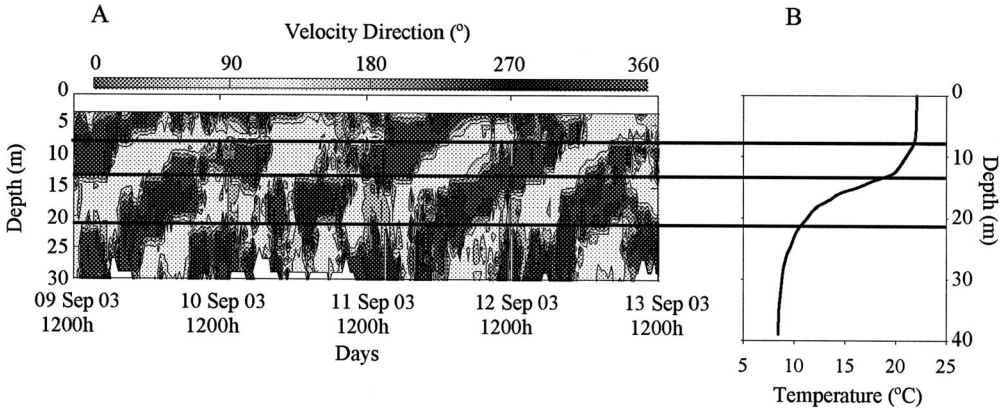

Fig. 4. (A) Velocity direction from the ADCP between 9 and 13 September 2003 and (B) vertical temperature profile on the 9 September 2003. The lines show the four layers present in the dynamic behavior. Values of water velocity have been averaged at one half–h periods.

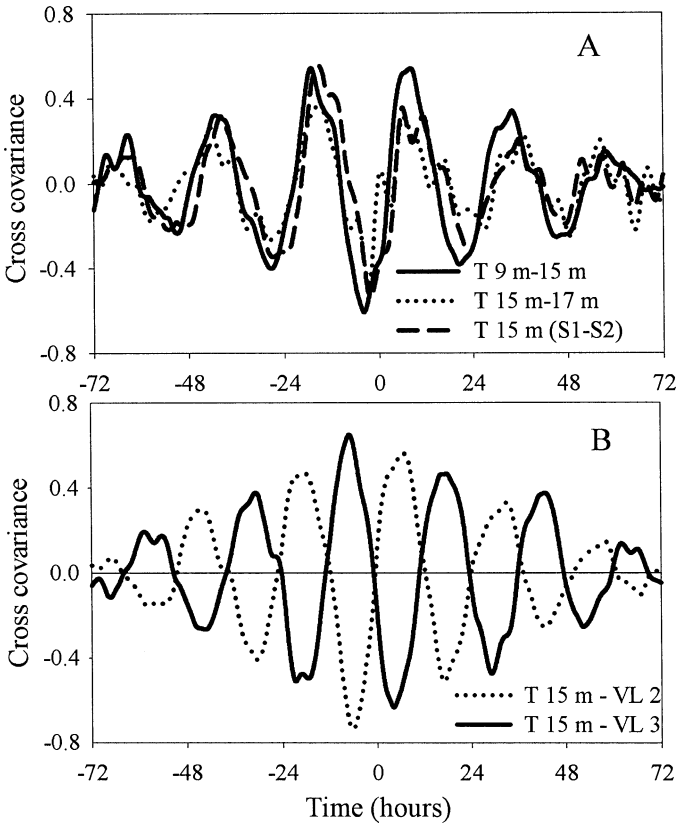

Fig. 5. Cross covariances normalized to one, for different time series. (A) Temperature at 9 and 15 m in depth at Sta. 1 (T9 m–15 m), temperature at 15 m and 17 m in depth at Sta. 1 (T 15 m–17 m), and temperature at 15 m in depth in at Sta. 1 and 2 (T15 m [S1–S2]). (B) Temperature at 15 m in depth and velocity in the layer 2 (T15 m–VL2) and temperature at 15 m in depth and velocity in layer 3 (T15 m–VL3).

opposite phase compared to the temperature at 15 m at Sta. 1 (Fig. 3E), indicating that a horizontal H1 mode may be excited (Fig. 1). To gain a better understanding of the temperature results, in Fig. 5A we represented the cross-covariance functions of the time series of the temperature at 15 m in depth at Sta. 1 compared with the temperature at 9 m and 17 m in depth at Sta. 1, and also with the temperature at 15 m in depth at Sta. 2. Note that for $t = 0$, the cross covariance is negative for all cases. Also note that, in spite of a certain delay, these time series with a 24-h period oscillate in phase. Figure 5B shows the cross covariance of the time series of velocity in layers two and three compared with the temperature at 15 m in depth at Sta. 1. This depth roughly corresponds to the interface between layers two and three. If the third mode oscillation occurs, one would expect that the velocity is at its maximum or minimum when the vertical displacements are zero. This would mean that the cross covariance should be close to 0 at $t = 0$, ± 12 h, ± 24 h, etc., and should be at its maximum or minimum at $t = \pm 6$ h, ± 18 h, ± 30 h, etc., which is approximately the pattern in Fig. 5B. All in all, these results indicate that a vertical V3H1 mode may have been occurring in Sau reservoir at the beginning of September 2003. To confirm this assessment, we will use a numerical model to calculate the eigenmodes for the Sau reservoir.

Numerical model—Although the stratification is often continuous, until recent years, modeling seiches has been confined mostly to two- or three-layer models, accounting for the epilimnion, metalimnion, and hypolimnion (Salvadé et al. 1988). Although these models are able to describe different horizontal modes, they can only describe a maximum of two vertical modes. However, increased computing power has allowed for the development of progressively more sophisticated internal seiche models that are able to resolve the internal standing waves produced by a continuous stratification profile, and, therefore, they can account for higher vertical modes (Múnnich 1996; Fricker and Nepf 2000; Antenucci and Imberger 2003).

The size of the Sau reservoir (Fig. 2), together with the fact that internal seiches are excited by the wind that blows through the canyon valley, made us think that the effects of the earth's rotation could be neglected. The internal Rossby radius of deformation $R_I = c/f$, where c is the phase speed of the internal wave and f the Coriolis parameter, represents the length scale over which Coriolis forces balance the pressure gradient generated by a tilted interface. Following Patterson et al. (1984), the criterion for the absence of rotational effects is $R = R_I/B > 1$, where B is the maximum width of the reservoir. If the reservoir length is L = 3,842 m and the period of the internal seiche for the V3H1 mode is T = 24 h, the phase speed can be estimated to be $c = 2L/T = 0.09$ m s^{-1}. Therefore, if $f = 1.02\ 10^{-4}$ s^{-1} and B = 700 m, we obtain $R_I \sim 880$ m and R = 1.25. Although slightly higher, this value is close enough to 1 to make us think that rotational effects cannot be discarded at the central part of the reservoir, where an internal Kelvin wave can be generated. However, because of the fact that the reservoir is elongated and only slightly narrower than R_I, the period of the Kelvin seiche should be almost identical to the seiche without rotation. At Sta. 1, where the reservoir width is small, the effect of the Kelvin mode is very similar to the effect that would have been caused by a mode without rotation and therefore we will not include rotational effects in the model.

The numerical model that we will use is similar to the one proposed by Múnnich (1996). In two dimensions, the governing equation for a stream function, ψ, of free, infinitesimal internal gravity waves in a hydrostatic Boussinesq fluid is

$$\frac{\partial^4 \psi}{\partial^2 t \partial^2 z} + N^2 \frac{\partial^2 \psi}{\partial x^2} = 0 \qquad (1)$$

where x and z are the horizontal and the vertical dimensions, t is time, $u = -\partial\psi/\partial z$ and $w = \partial\psi/\partial x$ are the horizontal and the vertical components of the velocity, and $N = N(z)$ denotes the Brunt–Väisälä frequency. Employing the rigid lid condition eliminates the surface waves. Then, assuming that there is no outflow at the boundaries, we get the condition $\psi = 0$. For seiches the time dependence has the following form: $\psi = \Phi(x, z)e^{i(\omega t+\sigma)}$, where ω is the angular frequency of the seiche and σ is a constant, which yields to the so-called generalized eigenvalue problem for the stream function Φ given by the equation

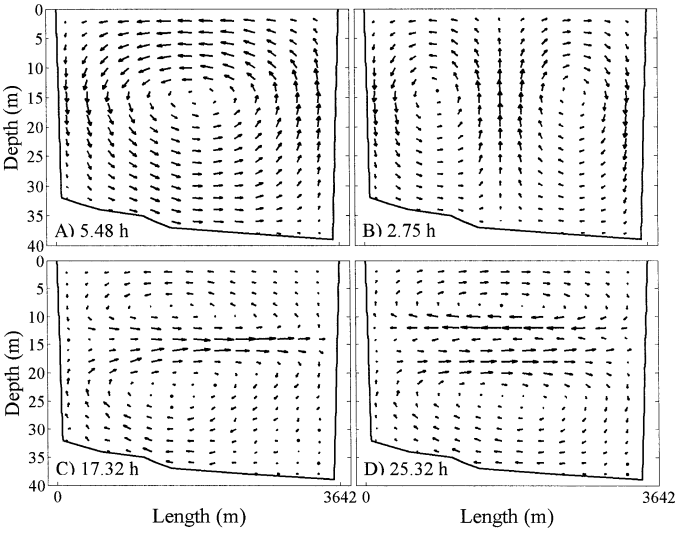

Fig. 6. Velocity field predicted by the model corresponding to modes (A) V1H1, (B) V1H2, (C) V2H1, and (D) V3H1. The corresponding predicted periods are (A) 5.48 h, (B) 2.75 h, (C) 17.32 h, and (D) 25.32 h, respectively.

$$\frac{\partial^2 \Phi}{\partial x^2} = \frac{\omega^2}{N^2} \frac{\partial^2 \Phi}{\partial z^2} \tag{2}$$

The domain was discretized, using centered finites differences, on a grid in which x follows the main axis of the reservoir; that way, along with the boundary conditions, the matrix formulation of the problem has the generalized eigenvalue form,

$$\mathbf{A}\Phi = \lambda \mathbf{B}\Phi \tag{3}$$

where **A** is a matrix determined by the discretization on the x axis and **B** a matrix determined by the buoyancy frequency and the discretization on the z axis. The origin $x = 0$ has been chosen at the position indicated in Fig. 2. The direction of the main axis of the reservoir makes a nearly 90° turn at the boundary $x = 0$. Visual observations of the wind and the surface waves show us that they drop to small values upstream of $x = 0$. Also, temperature measurements carried out with a thermistor chain show that temperature fluctuations due to internal waves are negligible. Because of this, we believe that the boundary will reflect the internal waves generated in the whole basin, although the veracity of this statement has to be confirmed by the model results. The set of solutions for λ, being $\lambda = \omega^2$, and Φ are the eigenvalues and eigenvectors of our generalized eigenvalue problem that we solve using the Jacobi–Davidson Method together with the so-called QZ algorithm (Bai et al. 2000). The Jacobi–Davidson method was used in the model to make it suitable for all grid sizes and all general cases. In the case of Sau, a 25×39 grid was used. Since the maximum depth for the period of September 2003 was 39 m, we needed to estimate the N^2 value for every meter depth.

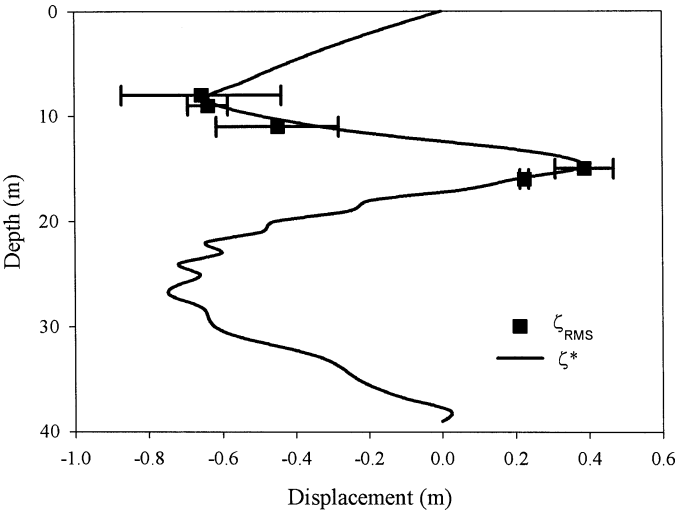

Fig. 7. Line: Variation of ζ^* (vertical displacement, ζ, obtained by the model multiplied by a constant α) with the depth at Sta. 1. Squares: Variation of ζ_{RMS} (RMS vertical displacement deduced from thermistor chain data) according to depth at Sta. 1. The bars indicate estimated error, which comes mainly from the determination of $\partial T/\partial z$.

The eigenmodes obtained were sorted by the overall shear connected to the flow field. The corresponding eigenvalues lead to the characteristic periods for the different modes. After Φ is obtained, the velocity components, u and w, follow easily. In Fig. 6 the velocity field together with the period obtained for the lowest modes, is represented. Although the solution was computed in a 26×39 grid mesh, for the sake of clarity, in Fig. 6 we have only represented the values over a 13×19 grid mesh. The temperature profile used corresponds to the 9 September 2003 (Fig. 4B). Given that the theoretical period obtained for the V3H1 mode is close to 24 h, we conclude that the observed oscillation corresponds to this mode.

To compare the model results to the thermistor chain observations, we have calculated the vertical fluid displacements from the model by using

$$\zeta = \int w \, dt = \frac{1}{i\omega} \frac{\partial \psi}{\partial x} = \frac{w}{i\omega} \tag{4}$$

As the used model is an eigenvalue model for the stream function, we are only interested in comparing the envelope of the seiche motion and not the absolute magnitude. Therefore, the value $(i\omega)^{-1}$ will be ignored. To determine seiche amplitude from the thermistor data, we follow the method proposed by Fricker and Nepf (2000), where a mean temperature profile $T(z)$ is first constructed by averaging the time series temperature profiles from the period 9 September–13 September. A root mean square (RMS) temperature deviation T_{RMS} is then computed for the predominant V3H1 mode in our system by using

$$\Delta T^i_{RMS} \equiv \sqrt{\frac{2}{N} \sum_{n=1}^{N} [T(z_i, t_n) - \bar{T}(z_i)]^2} \tag{5}$$

where

$$\bar{T}(z_i) = \frac{1}{N} \sum_{n=1}^{N} T(z_i, t_n)$$

N is the number of points in the thermistor data and z_i is the

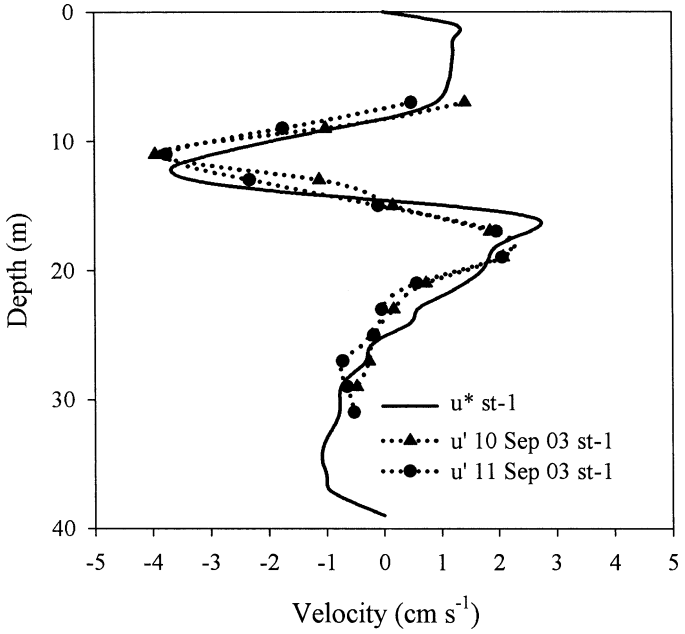

Fig. 8. Comparison between u^* (horizontal velocity obtained by the model multiplied by a constant β) and the maximum horizontal velocity obtained with the ADCP, u', for the dates: 10 September 2003 and 11 September 2003 at different depths in Sta. 1.

depth of the thermistor i. Finally, RMS vertical displacements are determined as

$$\zeta^i_{\mathrm{RMS}} = \frac{\Delta T^i_{\mathrm{RMS}}}{\partial \bar{T}/\partial z} \tag{6}$$

where the local gradient $\partial \bar{T}/\partial z$ is computed from the mean temperature profile $T(z)$. Note that the ΔT_{RMS} values obtained represent the absolute value of the wave envelope, and therefore, a study of the phase of the different time series, as shown in Fig. 5A, has been carried out in order to determine the sign of the vertical displacement.

Figure 7 compares the results of the maximum vertical displacements obtained from the model with the RMS vertical displacements from the thermistor chain at Sta. 1. Unfortunately, five thermistors were deployed in the surface mixed layer, and temperature gradients were too small to be used in Eq. 6; also, another thermistor was not operative during the measuring period, and therefore we were only able to use records from five thermistors. Notice that the envelope of the seiche obtained from the model fits the experimental results quite well. The maximum vertical displacements obtained by the model (ζ) have arbitrary units because the resultant eigenvectors of the model are not real velocity field vectors; in that sense, a constant, α, was used to fit experimental values to model results, so that $\zeta^* = \alpha\zeta$, where ζ^* values are represented in Fig. 7.

Likewise, we can compare the maximum horizontal velocity field obtained from the model with the maximum experimental velocity field obtained with the ADCP (Fig. 8). Once again, the velocity field obtained from the model has arbitrary units, and a constant β is used for comparison with the experimental data, where $u^* = \beta u$, and u is the horizontal velocity computed with the model. We have represented the maximum experimental velocities obtained on 10 and 11 September 2003. Note once again that the envelope of the seiche fits the experimental results quite well. It is important to point out the fact that the surface layer velocities are small compared to velocities in the second and third layers. Because of that, and the existence of the surface

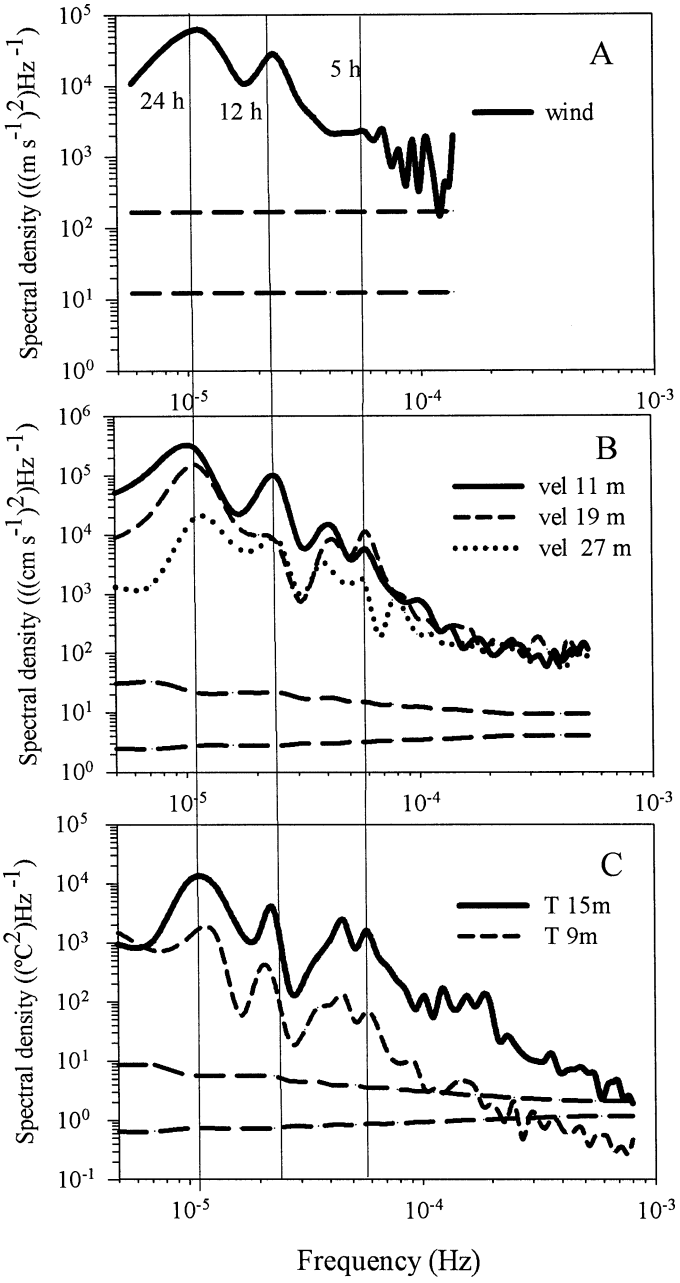

Fig. 9. (A) Power spectra density for the wind velocity, (B) velocity current, and (C) temperature series from 9–15 September 2003. Spectra in (B) and (C) have been smoothed in the frequency domain to improve confidence; dashed line shows confidence at the 95% level. Wind and velocity are projected following the mean axis of the reservoir. Continuous lines show the periods corresponding to the maximum peaks.

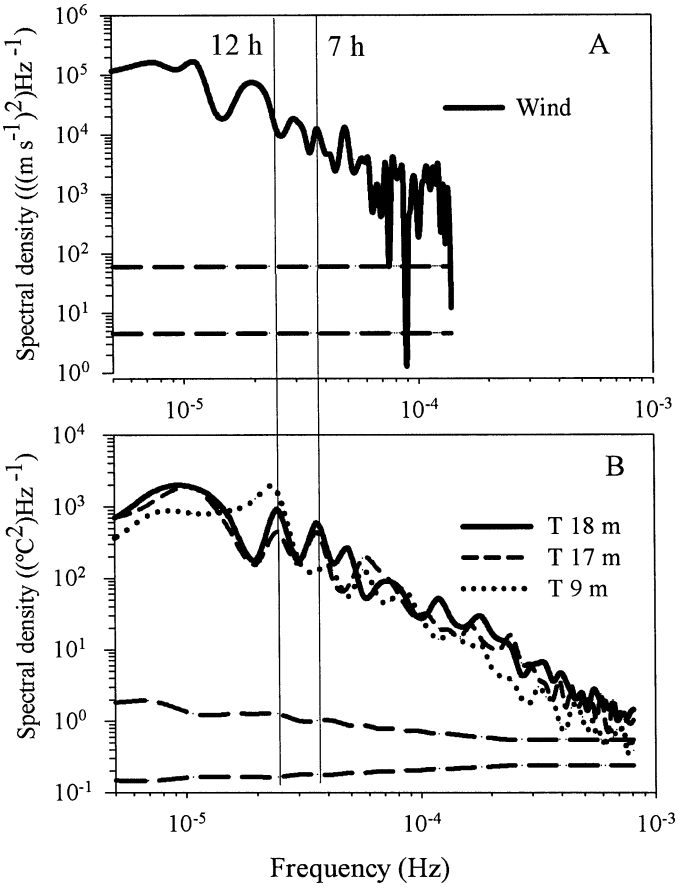

Fig. 10. (A) Power spectra density for the wind velocity and (B) temperature series from 21–31 July 2003. Spectra for the velocity have been smoothed in the frequency domain to improve confidence; dashed line shows confidence at the 95% level. Wind is projected following the mean axis of the reservoir. Continuous lines show the periods corresponding to the maximum peaks.

wind-driven current detected in Fig. 3B, the V3H1 mode is not clearly appreciated in the surface layer.

It is interesting to compare the spectral analysis for the period 9–15 September 2003 with the period 21–30 July 2003. In September 2003 (Fig. 9), the peak around 24 h appears in the time series for wind, velocity, and temperature. We attribute this peak to mode V3H1. However, the peak around 12 h that also appears in the time series does not correspond with the predicted modes (Fig. 6); this peak is probably the reservoir's response to a subdaily wind pattern. The 5-h peak in the velocity and temperature series does not have a corresponding peak in the time wind series. As the mode V1H1 has a period of ~5 h (Fig. 6), we attribute the peak to this mode. In normal conditions we would expect higher energy in mode V1H1, but the fact that mode V3H1 is resonant with the wind is probably causing the dampening of this mode. This can be corroborated by looking at the time series in July 2003 (Fig. 10). The temperature series show two peaks around 12 h and 7 h. The model calculations give periods of 6.2 h (V1H1), 11.7 h (V2H1), and 18.3 h (V3H1). Therefore, we attribute these peaks to modes V2H2 and V1H1.

All in all, when the metalimnion occupies a sufficiently large proportion of the water column, higher vertical modes may become excited by periodic winds. Such conditions are quite common in Mediterranean reservoirs at the end of the summer, when the mixed layer phenomena combined with the water being withdrawn create continuous stratification profiles. Given that continuous stratification profiles have a dense eigenfrequency spectrum, reservoirs can oscillate at many frequencies. Limitations on the oscillation modes will be imposed by the structure of the oscillation cells: thus, a higher number of cells, a greater attenuation of the mode. In Sau reservoir the presence of the V3H1 mode is obvious, especially from the current measurements. Resonance with the wind is a definitive contribution to the excitation of the V3H1 mode and in general to the higher modes. Typically the wind pattern has a period of ~24 h, and therefore, higher modes are excited when they have this periodicity.

References

ANTENUCCI, J. P., AND J. IMBERGER. 2003. The seasonal evolution of wind/internal wave resonance in Lake Kinneret. Limnol. Oceanogr. **48:** 2055–2061.

———, ———, AND A. SAGGIO. 2000. Seasonal evolution of the basin scale internal wave field in a large stratified lake. Limnol. Oceanogr. **45:** 1621–1638.

ARMENGOL, J., AND OTHERS. 1999. Longitudinal processes in canyon type reservoir: The case of Sau (N.E. Spain), p. 313–345. *In* J. G. Tundisi and M. Straskraba [eds.], Theoretical reservoir ecology and its applications. Backhuys Publishers.

BAI, Z., J. DEMMEL, J. DONGARRA, A. RUHE, AND H. VAN DER VORST. 2000. Templates for the solution of algebraic eigenvalue problems: A practical guide. SIAM.

CASAMITJANA, X., T. SERRA, C. BASERBA, AND J. PÉREZ. 2003. Effects of the water withdrawal in the stratification patterns of a reservoir. Hydrobiologia **504:** 21–28.

FRICKER, P. D., AND H. M. NEPF. 2000. Bathymetry, stratification, and internal seiche structure. J. Geophys. Res. **105:** 14237–14251.

GLOOR, M, A. WÚEST, AND M. MÚNNICH. 1994. Benthic boundary mixing and resuspension induced by internal seiches. Hydrobiologia **284:** 59–68.

IMBERGER, J. 1998. Flux path in a stratified lake: A review, p. 1–18. *In* Jorg Imberger [ed.], Physical processes in lakes and oceans. Coastal and Estuarine Studies, Am. Geophys. Union.

LAZERTE, B. D. 1980. The dominating higher order vertical modes of the internal seiche in a small lake. Limnol. Oceanogr. **25:** 846–854.

LEMMIN, U., AND C. H. MORTIMER. 1986. Tests of an extension to internal seiches of Defant's procedure for determination of surface seiche characteristics in real lakes. Limnol. Oceanogr. **36:** 187–192.

LEVI, D. A., R. L. JOHNSON, AND J. M. HUME. 1991. Shifts in fish vertical distribution in response to an internal seiche in a stratified lake. Limnol. Oceanogr. **36:** 187–192.

MACMANUS, J., AND R. W. DUCK. 1988. Internal seiches and subaqueous landforms in lacustrine cohesive sediments. Nature **334:** 511–513.

MÜNNICH, M. 1996. Influence of bottom topography on internal seiches in stratified media. Dyn. Atmos. Oceans **23:** 257–266.

———, A. WÚEST, AND D. M. IMBODEN. 1992. Observations of the second vertical mode of the internal seiche in an alpine lake. Limnol. Oceanogr. **37:** 1705–1719.

PATTERSON, J. C., P. F. HAMBLIN, AND J. IMBERGER. 1984. Classification and dynamic simulation of the vertical structure of lakes. Limnol. Oceanogr. **29:** 845–861.

PEREZ-LOSADA, J., E. ROGET, AND X. CASAMITJANA. 2003. Evidence of high vertical wave-number behaviour in a continuously stratified reservoir. J. Hydraulic Eng. **129:** 9734–9737.

ROGET, E., G. SALVADÉ, AND F. ZAMBONI. 1997. Internal seiche climatology in a small lake where transversal and second vertical modes are usually observed. Limnol. Oceanogr. **42:** 663–673.

SALVADÉ, G., F. ZAMBONI, AND A. BARBIERI. 1988. Three-layer model for the North Basin of the Lake of Lugano. Ann. Geophys. **6:** 463–474.

SPIEGEL, R. H., AND J. IMBERGER. 1980. The classification of mixed layer dynamics in lakes of small to medium size. J. Phys. Oceanogr. **10:** 1104–1121.

WIEGAND, R. C., AND V. CHAMBERLAIN. 1987. Internal waves of the second vertical mode in a stratified lake. Limnol. Oceanogr. **32:** 29–42.

WÜEST, A., AND A. LORKE. 2003. Small-scale hydrodynamics in lakes. Annu. Rev. Fluid Mech. **35:** 373–412.

———, G. PIEPKE, AND D. C. VAN SENDEN. 2000. Turbulent kinetic energy balance as a tool for estimating vertical diffusivity in wind-forced stratified waters. Limnol. Oceanogr. **45:** 1388–1400.

Received: 22 July 2004
Accepted: 4 January 2005
Amended: 12 February 2005